

Real-space spectral simulation of quantum spin models: Application to the Kitaev-Heisenberg model

Francisco M. O. Brito^{1*} and Aires Ferreira^{1†}

¹ Department of Physics and York Centre for Quantum Technologies,
University of York, York YO10 5DD, United Kingdom

* fmob500@york.ac.uk

† aires.ferreira@york.ac.uk

October 5, 2021

Abstract

The proliferation of quantum fluctuations and long-range entanglement presents an outstanding challenge for the numerical simulation of interacting spin systems with exotic ground states. Here, we present a Chebyshev iterative method that gives access to the thermodynamic properties and critical behavior of frustrated quantum spin models with good accuracy. The computational complexity scales linearly with the Hilbert space dimension and the number of Chebyshev iterations used to approximate the eigenstates. Using this approach, we calculate the spin correlations of the Kitaev-Heisenberg model, a paradigmatic model of honeycomb iridates that exhibits a rich phase diagram including a quantum spin liquid phase. Our results are benchmarked against exact diagonalization and a popular iterative method based on thermal pure quantum (TPQ) states. All methods accurately predict a transition to a stripy (spin-liquid) phase for the critical value of the Kitaev coupling $J_K \approx -1.3J_H$ ($J_K \approx -8.0J_H$) for honeycomb layers with ferromagnetic Heisenberg interactions ($J_H > 0$). Our findings suggest that a hybrid Chebyshev-TPQ approach could open the door to previously unattainable studies of quantum spin models in two dimensions.

Contents

1	Introduction	2
2	Chebyshev spectral methods: rationale	4
3	Methodology	5
3.1	Thermal Pure Quantum States	6
3.2	Chebyshev Polynomial Green Function	6
4	Applications: The Kitaev-Heisenberg model	8
4.1	Results: TPQ	9
4.2	Results: CPGF	10
5	Concluding Remarks	12

A Stochastic Trace Evaluation	14
References	14

1 Introduction

In strongly correlated materials, the interplay between different types of interactions can conspire to produce rich $T = 0$ phase diagrams characterized by a series of transitions between paramagnetic, magnetically ordered and quantum spin liquid phases. These quantum phase transitions are driven by one or more parameters in the Hamiltonian, such as an external magnetic field or a spin exchange coupling constant. When a drastic change in the ground state occurs as one of these parameters is varied, there is an accompanying change in the thermodynamic properties. This change manifests itself in the form of critical behavior of quantities such as the structure factor and the susceptibility, which scale with the parameter that drives the transition [1, 2].

The study of the subtle competition between quantum fluctuations and interactions at the heart of quantum phase transitions often calls for a numerical approach [3–9]. Exact solutions are only known for a handful of cases (a well-known example is the isotropic Heisenberg chain in one dimension [10]). Moreover, in low dimensions, the presence of strong quantum fluctuations limits the applicability of mean-field approaches. Exact diagonalization (ED) methods, such as those based on the Lanczos algorithm [11], are the next step beyond exact analytical solutions. There are several examples of the application of this method to interacting spin systems, for example Refs. [3, 9, 12]. Unfortunately, these are limited to relatively small system sizes, even when codes are optimized so as to include eventual symmetries of the model. The culprit is the exponential scaling of the computational cost with the system size, which is particularly severe in dimensions greater than one. In an attempt to go beyond this limitation of ED, several numerical techniques have been deployed with varying degrees of success, including series expansions [13–19], quantum Monte Carlo (QMC) [5, 6, 20], density matrix renormalization group (DMRG) [21–23] and thermal pure quantum (TPQ) states [24–27].

The most efficient numerical schemes amenable to large-scale computations share a key feature: they aim at reconstructing expectation values of quantum observables without having to fully diagonalize the Hamiltonian. The resulting computational cost depends crucially on how the expectation values of the observables are evaluated. Here, two relevant aspects are at play. The first has to do with how the corresponding operators are reconstructed. The second relates to the process by which one obtains the expectation value. Usually this process is a stochastic one, unless there is prior knowledge about some of the system’s features, in which case a variational approach can be viable [20, 28, 29].

In principle, QMC methods can be used to probe large systems in any number of dimensions, while remaining numerically exact [5, 6]. However, they are plagued by the sign problem [30]. This is a situation where the variance of the estimators of quantities of interest increases exponentially due to quantum statistics. The severity of the problem depends on the nature of the correlations in the model. Generally, the sign problem tends to be more acute in frustrated systems, hampering the use of QMC to extract quantities of interest, such as correlation functions. The sign problem and the limited range of models that QMC is able to access emphasize the need

for a general purpose method that can be used more broadly as an alternative to ED and QMC.

In this work, we apply a general-purpose iterative method based on Chebyshev polynomial expansions to compute spin correlations with controlled accuracy in a paradigmatic frustrated system with competing (Kitaev and Heisenberg) interactions. The Kitaev model on the honeycomb lattice is one of the rare examples of an exactly solvable microscopic model [31] showing exchange frustration, i.e. nearest neighbor interactions that cannot be simultaneously minimized. This is similar to geometric frustration which notably occurs in the case of the antiferromagnetic Ising model on the triangular lattice [32]. In the Kitaev case, frustration is created by bond-directional interactions which give way to a fractionalized excitation spectrum of Majorana fermions. The physical realization of the Kitaev model has attracted great attention because it opens up the possibility of synthesizing spin liquid materials with exotic topological orders [33, 34]. Notably, in honeycomb iridates, which are transition metal oxides with partially filled d-shells, a subtle interplay of spin-orbit coupling and electronic correlations produces the type of bond-directional interactions that appear in the Kitaev model. Thus, these materials make good spin liquid candidates. In these spin-orbit assisted Mott insulators, the Kitaev exchange interaction is thought to be responsible for the emergence of a spin liquid phase [3, 33, 35–37].

The Kitaev exchange interaction also plays a key role in the modelling of other compounds such as the van der Waals ruthenate α -RuCl₃. A recent relevant example is a study that proposes a minimal microscopic 2D spin model for α -RuCl₃ [38]. The model at play is an extension of the Kitaev model that considers both Kitaev and Heisenberg exchange interactions, third neighbor exchange and Γ interactions (i.e., terms that couple different spin components for each nearest neighbor bond). The authors treat this generalized Kitaev-Heisenberg (K-H) model using a mean-field random-phase approximation, aiming at extracting quantities such as the dynamical structure factor [38]. The use of this mean-field approach is justified by comparing its results with those of exact diagonalization [12]. However, exact diagonalization is limited to relatively small system sizes (for example, in Ref. [12], the authors use a 24-site cluster). Thus, this approach runs into the risk of overlooking large scale properties of the model. In fact, in Refs. [39, 40], the authors detect small finite-size effects when computing the dynamical spin structure factor using QMC simulations of the Kitaev model in the presence of disorder — which deems the study of large scale properties crucial — even for clusters of 288 sites¹. These developments illustrate the need to develop accurate, general purpose computational methods that scale favorably with the system size.

This work is organized as follows. Section 2 provides a bird’s-eye view of the Chebyshev polynomial-based spectral approach and its applications in condensed matter physics. In Sec. 3 we give details of the techniques used throughout this study: the microcanonical variant of the TPQ (Sec. 3.1) and the iterative Chebyshev Polynomial Green’s function (CPGF) method (Sec. 3.2). We discuss the convergence properties in detail and close the section by briefly comparing the performance of the two approaches (CPGF and TPQ). In Sec. 4 we use these methods to compute the ground state and nearest-neighbor spin-spin correlation function of the K-H model and compare our findings with existing results obtained with the ED technique. We present a detailed analysis of the dependence of our estimators for the spin-spin correlation on the relevant parameters: the number of initial random states, truncation order and, in the case of the CPGF, also the energy resolution. Finally, in Sec. 5, we point out the pros and cons of each method. In particular, we emphasize the additional control gained by specifying the energy resolution directly

¹Note that the Monte Carlo approach of Refs. [39, 40] requires the partial diagonalization of the original Hamiltonian in terms of Majorana fermions. On the other hand, a direct Quantum Monte Carlo simulation of the Kitaev model suffers from the sign problem.

in CPGF and we explain in which situations this additional control could prove useful. Possible extensions of this work are highlighted.

2 Chebyshev spectral methods: rationale

The Chebyshev polynomial-based spectral method is an increasingly popular tool in the simulation of many-body systems that fulfills the requirement of general applicability [41–53]. It relies on the iterative spectral reconstruction of the target functions of interest (e.g., density of states and spin–spin correlations). The iterative scheme is stable and can be made as accurate as required within the specified energy resolution. Unlike ED—which relies on the knowledge of individual states and therefore is limited to very small systems—the spectral approach uses a coarse-grained description of energy states to provide estimates for quantum observables in large systems (see Fig. 1). In practical implementations, spectral methods take advantage of a stochastic computation of the moments of the polynomial expansion to further reduce the computational cost and are amenable to parallelization.

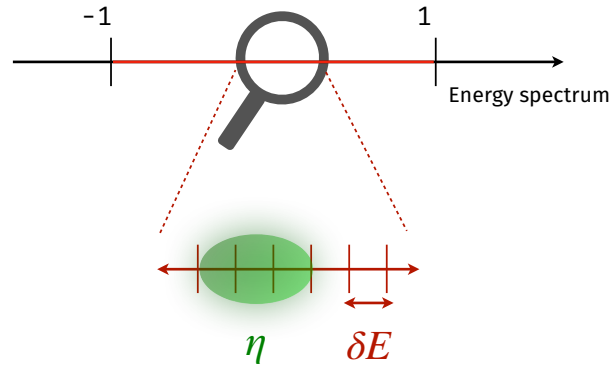


Figure 1: In the spectral approach, the energy spectrum is probed using a coarse-grained average of energy states within the required energy resolution η .

The technique we based this work upon [54, 55] has proven to be very effective in dealing with tight-binding models, allowing unprecedented large-scale simulations with billions of atomic orbitals [54, 56]. Our aim here is to show that such a real-space spectral approach can be used on its own (or combined with TPQ), with various degrees of approximation, to explore the low-temperature properties of two-dimensional quantum spin models.

The efficient evaluation of Chebyshev moments relies on estimators for expectation values that exploit random vectors² to evaluate traces of operators [57]. The idea is to approximate the trace of an operator by an average of expectation values in random vectors, i.e. $\text{Tr}_{\text{STE}} \hat{O} := \frac{1}{N_{\text{rd.vec.}}} \sum_{r=1}^{N_{\text{rd.vec.}}} \langle r | \hat{O} | r \rangle$. The relative error scales favourably with the Hilbert space dimension ($\propto 1/\sqrt{D}$) and, for a fixed system size, can be made as small as desired by increasing the number of random vectors. This technique, dubbed stochastic trace evaluation, is ubiquitous in the study of condensed phases and is used in ED methods, such as those based on the Lanczos algorithm, in the method of thermal pure quantum states [24, 25], and in the kernel polynomial method [41].

²A random vector is defined as $|r\rangle = \sum_{i=1}^D \xi_i |i\rangle$, with $\{|i\rangle\}$ an arbitrary basis and $\xi_i \in \mathbb{C}$ random variables that satisfy $\overline{\xi_i} = 0$, $\overline{\xi_i \xi_j} = \delta_{ij}$ and $\overline{\xi_i^* \xi_j} = \delta_{ij}$ (here the bar denotes statistical average).

Stochastic trace estimators are a crucial advantage with respect to QMC because these estimators are free from the sign problem. Another crucial feature of the spectral approach is that it approximates target functions with uniform resolution over the full spectral range (and in the case of CPGF the resolution can be specified exactly). This is a key aspect in the study of phase transitions, particularly when one wishes to characterize the critical behavior of thermodynamic functions. There are two ways to define an energy resolution. One of them uses a kernel that is convoluted with the function that one wishes to expand in Chebyshev polynomials. In practice, this convolution leads to a modification in the coefficients of the expansion. This modification smears out so called Gibbs oscillations which occur upon truncation of the Chebyshev series near discontinuities of the target function. These oscillations lead to a loss of precision and increased fluctuations, which are circumvented by convolution with an appropriate kernel [41]. Within this approach, the resolution is defined as the spread of the kernel in the xy -plane, and generally depends on the truncation order and energy. Here, instead, we use a Chebyshev decomposition of broadened lattice Green's functions that was proposed independently in the works of Ferreira and Mucciolo [54] and Braun and Schmitteckert [55]. This approach, coined CPGF [54], has two main features: (i) it is based on a stable, asymptotically exact expansion of lattice Green's functions; and (ii) the energy resolution is specified from the outset and is uniform over the full spectral range.

On the other hand, TPQ approximates the ground state by successive application of the Hamiltonian operator onto an initial random state. In TPQ, the number of iterations is proportional to a quantity that plays the role of an effective temperature in analogy with thermal annealing. Broadly speaking, this effective temperature plays the role of a resolution that becomes finer as more iterations are completed.

In the following sections, we will compare the two methods since they both scale linearly with the dimension of the Hilbert space D with all other parameters being fixed. Moreover, both methods scale linearly with the number of polynomials required for spectral convergence (or iterations in the case of TPQ) $N_{\text{poly/it}}$, and with the number of realizations of the initial random state required for statistical convergence $N_{\text{rd.vec.}}$. The recent interest in these methods stems from the emerging trend in numerical simulations that combines stochastic trace evaluation of operators with highly efficient recursive approximations of spectral operators and Green's functions [26, 27, 44, 47, 48, 51–53, 56, 58, 59].

3 Methodology

The methods described in this section involve two main steps. First, an approximate spectral representation of the target state (e.g., the ground state) is obtained with polynomial computational complexity. This is achieved by recursively applying the Hamiltonian on an initial random state. After such quasi-eigenstate is found, the physical observable is computed by acting with the corresponding string of operators on the reconstructed state. Equivalently, one may regard this first step as a reconstruction of the relevant operator restricted to the desired energy shell. The second step then boils down to computing averages over random states drawn from the Hilbert space. The reconstructed operator will automatically restrict these to the relevant energy (with a pre-defined resolution in the case of CPGF).

3.1 Thermal Pure Quantum States

In this section, we follow closely the work of Sugiura and Shimizu [24]. The rationale of the TPQ method is to find a pure state that faithfully captures the equilibrium properties of a quantum system at finite temperature as accurately as possible. A TPQ state is constructed as follows. First, one generates a random state

$$|\psi_0\rangle \equiv \sum_{i=1}^D \xi_i |i\rangle. \quad (1)$$

For simplicity, $\{|i\rangle\}$ is usually taken as the set of products states of individual spins. The distribution of energy in $|\psi_0\rangle$ is proportional to the density of states

$$g(u; N) = \exp[Ns(u; N)], \quad (2)$$

where $s(u; N)$ is the entropy density, which converges to the N -independent one $s(u; \infty)$ as $N \rightarrow \infty$, where N is the number of sites on the lattice [24].

The basic procedure is an iterative one similar to minimization annealing schemes. The goal is to modify the distribution of energy in the random state so that it becomes sharply peaked at the desired energy E . This is achieved by operating with a suitable polynomial of the Hamiltonian normalized to the number of sites on the lattice $\hat{h} = \hat{H}/N$ onto $|\psi_0\rangle$ iteratively. Take a constant $l \sim \mathcal{O}(1)$, such that $l \geq e_{\max}$, where e_{\max} is the maximum eigenvalue of the Hamiltonian normalized to the number of sites. Start from $|\psi_0\rangle$ and compute, respectively the energy density and the new state

$$u_k = \langle \psi_k | \hat{h} | \psi_k \rangle, \quad |\psi_{k+1}\rangle \equiv \frac{(l - \hat{h}) |\psi_k\rangle}{\|(l - \hat{h}) |\psi_k\rangle\|} \quad (3)$$

iteratively for $k = 1, 2, \dots, N_{\text{it}}$, the maximum number of iterations. Later, we will see that N_{it} plays a role analogous to the inverse of the resolution in the Chebyshev expansion.

The first energy density corresponds to the infinite temperature state at $\beta = 0$. Thus, $g(u; N)$ has its maximum at $u = u_0$. Then, the energy density decreases gradually towards the ground state energy e_{\min} as k is increased: $u_0 > u_1 > \dots > u_{N_{\text{it}}} \geq e_{\min}$. One stops iterating at $k = N_{\text{it}}$, when u_k gets close enough to the ground state energy for our purposes.

At finite temperature, $N_{\text{it}} \propto N$ and $|\psi_0\rangle, |\psi_1\rangle, \dots, |\psi_{N_{\text{it}}}\rangle$ is a sequence of TPQ states corresponding to decreasing energy densities $u_0 > u_1 > \dots > u_{N_{\text{it}}}$. Thus, an estimate of the equilibrium value of an arbitrary observable \hat{A} is obtained as $\langle \psi_k | \hat{A} | \psi_k \rangle$ as a function of u_k . Correspondingly, an effective temperature (T_{eff}) may be obtained [24]. For each realization of the coefficients $\{c_i\}$, $\langle \psi_k | \hat{A} | \psi_k \rangle$ depends exponentially less on the number of sites N as the latter is increased due to self averaging properties. Hence, accurate results are often obtained with a few or even a single random vector realization [24, 25].

3.2 Chebyshev Polynomial Green Function

This method consists of numerically evaluating the lattice resolvent operator via an exact expansion in terms of Chebyshev polynomials of the Hamiltonian matrix

$$\hat{G}(z) = (z - \hat{H})^{-1} \quad (4)$$

with $z = E + i\eta$ a complex energy variable. A key aspect is that the Green's function is reconstructed with uniform resolution over the entire energy range. For numerical stability, the resolution parameter should satisfy $\eta = \text{Im} z \gtrsim \delta E$, where δE is the mean level spacing. To expand Eq. (4) into Chebyshev polynomials, we rescale the Hamiltonian and the energy variables according to $\tilde{z} = \varepsilon + i\lambda$ and $\tilde{H} = (\hat{H} - b)/a$. Here, $\varepsilon = (E - b)/a$ and $\lambda = \eta/a$, and

$$a = f \frac{E_{\max} - E_{\min}}{2} \quad b = \frac{E_{\max} + E_{\min}}{2}, \quad (5)$$

where E_{\max} and E_{\min} are the extremal eigenvalues and $f \simeq 1.01$ is a safety factor to ensure numerical stability. As customary, we work with Chebyshev polynomials of the first kind $\{T_n(x) = \cos(\arccos nx)\}$ due to their favorable convergence properties [60].

Target functions of energy are evaluated by expressing the Green's function in terms of an exact polynomial expansion [54] in the rescaled Hamiltonian \tilde{H} , as follows

$$\hat{G}(\varepsilon + i\lambda) = \sum_k \frac{\lambda}{(\varepsilon - \varepsilon_k)^2 + \lambda^2} |k\rangle \langle k| = \sum_{n=0}^{\infty} g_n(\varepsilon, \lambda) T_n(\tilde{H}), \quad (6)$$

with

$$g_n(z) = \frac{-2i}{1 + \delta_{0,n}} \frac{(z - i\sqrt{1-z^2})^n}{\pi\sqrt{1-z^2}}. \quad (7)$$

The operators $T_n(\tilde{H})$ of Eq. (6) are constructed using the operator versions of the Chebyshev recursion relation

$$\begin{aligned} T_0(\tilde{H}) &= 1, \\ T_1(\tilde{H}) &= \tilde{H}, \\ T_{n+1}(\tilde{H}) &= 2\tilde{H}T_n(\tilde{H}) - T_{n-1}(\tilde{H}). \end{aligned} \quad (8)$$

The series is truncated when the desired accuracy is achieved. The N_{poly} -th order approximation of the lattice Green's function is therefore

$$\hat{G}_{N_{\text{poly}}}(\varepsilon + i\lambda) := \sum_{n=0}^{N_{\text{poly}}-1} g_n(\varepsilon, \lambda) T_n(\tilde{H}). \quad (9)$$

We note that, as a rule of thumb, $N_{\text{poly}} = a\lambda^{-1}$, with $a = O(1)$, suffices to achieve machine precision in most cases [56].

The spectral operator within the CPGF approach can be defined as follows

$$\delta_\lambda(\varepsilon - \tilde{H}) = - \sum_n \text{Im}[g_n(\varepsilon + i\lambda)] T_n(\tilde{H}). \quad (10)$$

By applying this operator to a random state $|r\rangle$, we obtain $|\psi_r(\varepsilon, \lambda)\rangle$, a state with energy ε (within the resolution λ). Finally, expectation values are computed according to

$$A_r(\varepsilon, \lambda) := \frac{\langle \psi_r(\varepsilon, \lambda) | \hat{A} | \psi_r(\varepsilon, \lambda) \rangle}{\langle \psi_r(\varepsilon, \lambda) | \psi_r(\varepsilon, \lambda) \rangle}. \quad (11)$$

Provided that the resolution λ is adequate ($\lambda \rightarrow \delta\varepsilon^+ \equiv \delta E/a$, where δE is the mean level spacing), one obtains an accurate estimate of the expectation value of \hat{A} for a given energy ε , according to

$$A_{\text{CPGF}}(\varepsilon, \lambda) := \frac{1}{N_{\text{rd.vec.}}} \sum_{r=0}^{N_{\text{rd.vec.}}-1} A_r(\varepsilon, \lambda) \xrightarrow{\lambda \rightarrow \delta\varepsilon^+} A(\varepsilon). \quad (12)$$

As we shall in a concrete case see below, the standard deviation of this estimator is generally proportional to $N_{\text{rd.vec.}}^{-1/2}$ [57].

4 Applications: The Kitaev-Heisenberg model

In this section we apply the methods described in Sec. 3 to the K-H model on a 4×3 honeycomb lattice with periodic boundary conditions. We recover the results of Ref. [3] using three methods: ED (as used in the original reference), TPQ and CPGF, thereby showing that the latter is a viable alternative for the study of frustrated quantum magnets.

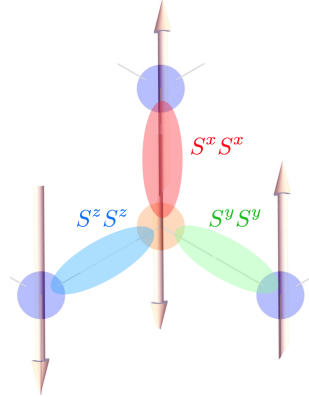


Figure 2: Nearest neighbor bonds on the honeycomb lattice colored in red, green and blue (respectively $\gamma = x, y, z$ in our cartoon). The bond-directional character of the Kitaev interaction implies that to each bond corresponds a different type of interaction. Similarly to the case of the Ising model on the triangular lattice, where we have geometrical frustration, here we have exchange frustration due to the nature of the interaction and it is not possible to find a spin configuration that simultaneously minimizes the energy on all links.

The K-H model combines Kitaev and Heisenberg interactions. For each nearest neighbor bond $\langle i, j \rangle$ on the honeycomb lattice, one has

$$\begin{aligned} \hat{H}_{\text{Kit. } ij}^{(\gamma)} &= J_K \hat{S}_i^\gamma \hat{S}_j^\gamma, \\ \hat{H}_{\text{Heis. } ij} &= J_H \hat{\mathbf{S}}_i \cdot \hat{\mathbf{S}}_j \end{aligned} \quad (13)$$

with $J_K = -2\alpha$, $J_H = 1 - \alpha$ and where $\gamma = x, y, z$ is one of the three types of bond on the honeycomb lattice. Here, $\alpha \in [0, 1]$ parameterizes the strength of each term. The Kitaev interaction is bond-directional, i.e. for each distinct type of bond $\gamma = x, y, z$, there is a correspondent interaction

(respectively $S^x S^x$, $S^y S^y$, $S^z S^z$), as shown in Fig. 2. The Hamiltonian can be cast as a sum over nearest neighbor bonds $\langle i, j \rangle^\gamma$ (the superscript refers to the type of bond) on the honeycomb lattice:

$$\hat{H} = \sum_{\langle i, j \rangle^\gamma} \left(\hat{H}_{\text{Heis. } ij} + \hat{H}_{\text{Kit. } ij}^{(\gamma)} \right). \quad (14)$$

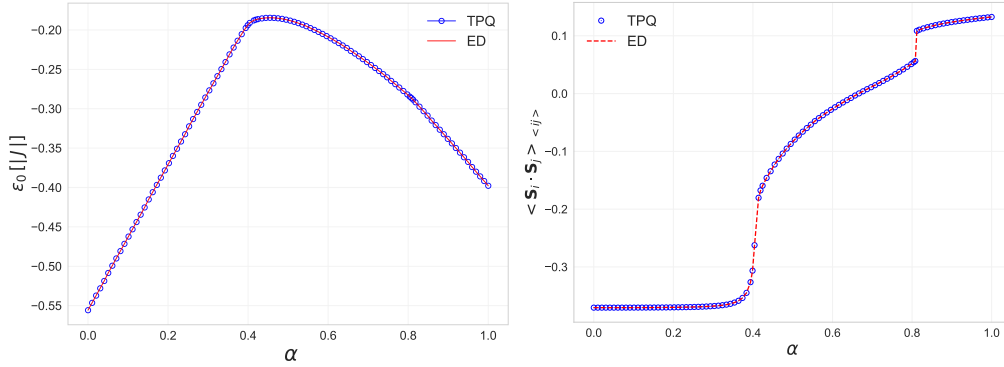


Figure 3: Left panel — Comparison between the ground state energy of a 24-site Kitaev-Heisenberg model on the honeycomb lattice (4×3 lattice with periodic boundary conditions) using both the TPQ method and ED. The two curves show excellent agreement. Right panel — Ground state nearest neighbor spin–spin correlation computed with TPQ compared with the ED result. In this TPQ calculation, we used 40000 iterations and 4 realizations of the initial random state.

For each value of α , we computed the ground state energy using an ED technique (Lanczos algorithm). Then, we used this energy as an unbiased input for the Chebyshev expansion. The ground state energy can also be accurately estimated using TPQ; this is shown in Fig. 3 (left panel). This is because TPQ achieves its maximum effective resolution at low temperatures (i.e. large N_{it}) where it accurately approximates the ground state and low-lying excitations [24, 25, 27, 61]. In what follows, we present our results for the nearest-neighbor correlator of the K-H model computed with the different methods.

4.1 Results: TPQ

We focus the subsequent discussions on the nearest-neighbor correlation function of the K-H model. In Fig. 3 (right panel), we obtain remarkable agreement between the spin–spin correlation computed with ED and TPQ. We used 4 realizations of the initial random state across the entire phase diagram. As mentioned in Sec. 3.1, this suffices due to the self-averaging properties of the TPQ estimator. TPQ is designed to accurately estimate the ground state energy via an iterative procedure. Thus, it is perhaps not too surprising that the nearest-neighbor spin correlation function is computed with comparable accuracy. Note that near the isotropic, Heisenberg point ($\alpha = 0$) these two quantities are in fact exactly related. Our simulations show that convergence (with respect to N_{it}) is generally fast. However, as we approach the Kitaev limit ($\alpha = 1$), the converge of the TPQ estimator for the spin–spin correlation slows down notoriously. As the Kitaev term on the Hamiltonian becomes dominant ($|J_K|/|J_H| \gg 1$), the ground state energy per site ϵ_0

and the nearest neighbor spin–spin correlation $\langle \mathbf{S}_i \cdot \mathbf{S}_j \rangle_{\langle ij \rangle}$ start to differ significantly. Hence, close to the spin liquid critical point (e.g., $\alpha \simeq 0.8 \iff |J_K|/|J_H| \simeq 8$), the computational effort grows substantially, with TPQ requiring about 40000 iterations for convergence to occur satisfactorily. This point will be addressed in detail below when contrasting TPQ with CPGF.

4.2 Results: CPGF

Next, we present the results obtained with the CPGF approach. We start by establishing the accuracy of the stochastic trace evaluation of Eq. (12). A detailed analysis shown in Appendix A confirms that the standard deviation of the estimate for the nearest-neighbor spin–spin correlation function scales as predicted, i.e. as the inverse square root of the number of realizations of the initial random state.

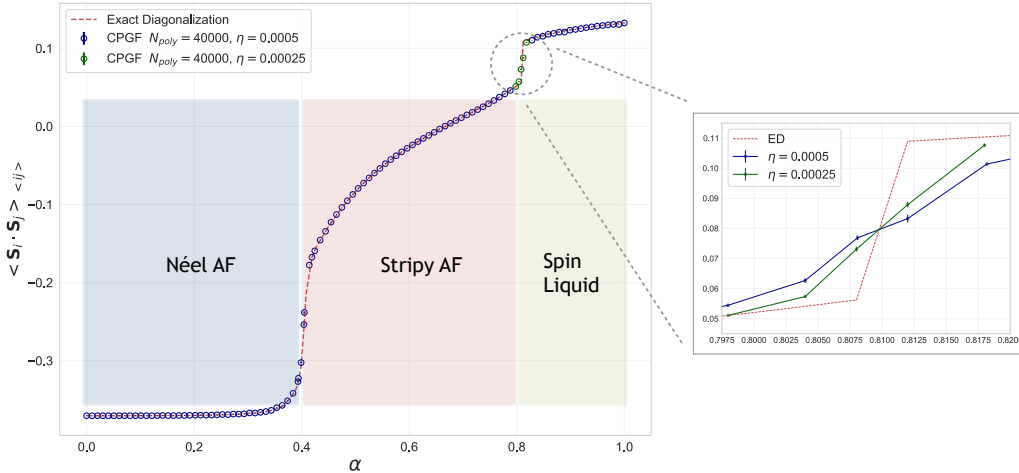


Figure 4: Ground-state spin–spin correlation function of the K-H model. The data represented by the dots were obtained using the CPGF method. The error bars are smaller than the size of the dots except at the phase transitions located at $\alpha \simeq 0.4$ and $\alpha \simeq 0.8$. The red dashed line shows our ED results (first reported in Ref. [3]). Inset: Close up of the transition to the spin liquid phase at $\alpha \sim 0.8$. These results were obtained with two different energy resolutions (in units of the coupling constant J_H). Statistical fluctuations are enhanced in the case of the finer resolution ($\eta = 0.00025J_H$). Error bars in the inset were estimated using 40-60 independent random vector realizations.

Figure 4 shows the correlation function of a 24-site cluster across the phase diagram calculated with the CPGF approach. As discussed in Ref. [3], the steps signal two quantum phase transitions i.e., from a Néel antiferromagnet to a stripy antiferromagnetic phase (at $\alpha \simeq 0.4$) and from stripy antiferromagnetic phase to a spin liquid (at $\alpha \simeq 0.8$).

To assess the spectral convergence in the K-H model, for any given resolution, we carefully track the evolution of the correlation function with N_{poly} in Eq. (9). In Fig. 5, we show this behavior for energy resolution $\eta = 0.0005J_H$ for a spread of α -values in the interval $[0, 1]$. As it turns out, good convergence is already achieved for $N_{\text{poly}} \sim 20000$ for all values of α . This suggests that with the highest truncation order in our simulations (i.e., $N_{\text{poly}} = 40000$), one could in fact probe the system with energy resolutions approximately improved by a factor of 2. An enhanced

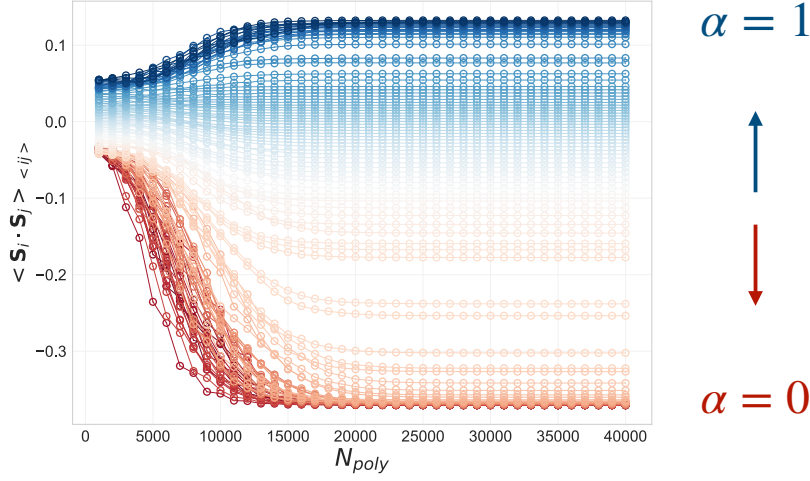


Figure 5: Spectral convergence for $\eta = 0.0005J_H$. Each color represents a different value of α as per the legend on the right.

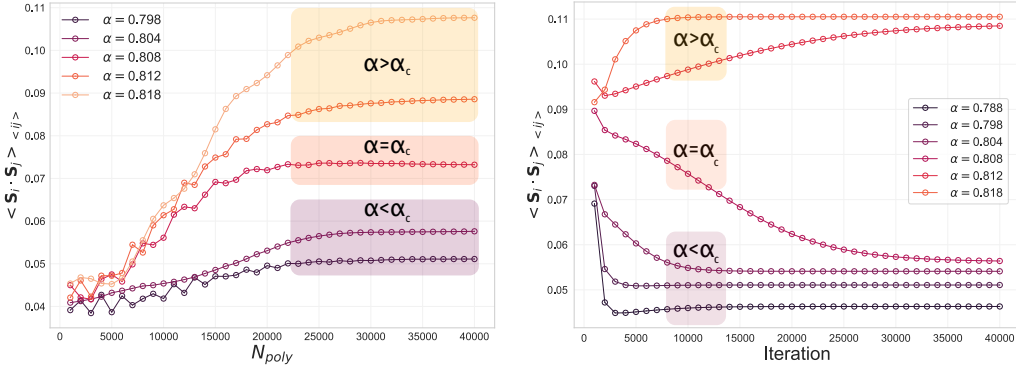


Figure 6: Left panel — Spectral convergence near criticality for a resolution $\eta = 0.00025J_H$. At the critical point $\alpha = 0.808$, the required number of polynomials is similar to the number of iterations required by TPQ. Right panel — Convergence of the TPQ estimator. The x -axis shows the number of iterations used in the scheme described in Eq. (3). We chose representative values of α to illustrate convergence. Note that convergence is particularly slow for $\alpha = 0.808$, i.e. at the critical point for the transition to the spin liquid phase.

resolution is particularly important in the vicinity of a quantum critical point, as illustrated in the inset of Fig. 4.

A close up of the spectral convergence near the transition to a spin-liquid phase is reported in Fig. 6. First, we confirm that we obtain spectral convergence at the critical point $\alpha_c = 0.808$ with the finest simulated energy resolution ($\eta = 0.00025J_H$) (see Fig. 6 left panel). The curve illustrating this is shown in red. The convergence gets progressively slower as one approaches the quantum critical point from lower values ($\alpha < \alpha_c$, shown in Fig. 6 in purple). Remarkably, the convergence slows further in the quantum spin liquid phase ($\alpha > \alpha_c$, shown in Fig. 6 in orange). Convergence is established when the estimator shows no appreciable changes when more

polynomials are added to the CPGF expansion. Graphically, the spin–spin correlation flattens as more polynomials are considered.

The right panel of Fig. 6 shows the equivalent convergence of the TPQ estimator for the same values of α . By comparing the two panels of Fig. 6, we conclude that close to the phase transition to the spin liquid phase at $\alpha \sim \alpha_c$ the two methods require roughly the same number of polynomials/iterations to achieve convergence (30000-40000). Here we consider the finest resolution for the CPGF calculation ($\eta = 0.00025J_H$). In the TPQ calculation, convergence is particularly slow at the critical point and comparatively faster for $\alpha < \alpha_c$ and $\alpha > \alpha_c$, whereas in CPGF the convergence speed is similar for all values of α around the critical point. Notably, using TPQ, the point we considered within the spin liquid phase closest to the transition ($\alpha = 0.812$) still shows slow convergence (similar to that of the critical point).

We close this section with a note on computational cost. Our calculations were done using Intel Xeon Gold 6138 processors running at 2 GHz. Each simulation required 70 GB of memory and about 1.5h per core per random vector using 40000 polynomials. In this work, we used a simple code to assess the viability of CPGF in two-dimensional systems of interacting quantum spins. We expect that by implementing a multi-domain parallelization scheme as in the KITE code [56], we could reduce the memory requirement to a few GB and achieve systems with 34–36 spins (i.e., similar Hilbert space dimension to the tight-binding systems with 10^{10} orbitals demonstrated in Ref. [56] using KITE). Such an optimized implementation could enable the exploration of even larger systems currently only accessible by DMRG and QMC [7, 39, 62–65].

5 Concluding Remarks

We studied the Kitaev-Heisenberg model on a 4×3 honeycomb lattice with periodic boundary conditions using three distinct approaches. We started by reproducing the results of Ref. [3] using exact diagonalization. Then, we recovered those results using TPQ and Chebyshev expansions (CPGF), independently. For these two methods, we carefully examined the spectral and statistical convergence properties.

In terms of computational effort, calculations with a 24-spin cluster are relatively modest for both methods. We focused on this relatively small system so that we could reliably compare our results with the ones obtained with ED, which we used as a control method. Another important remark is that TPQ is designed to minimize the ground state energy, which in this case is closely related to the observable we focus on (the nearest neighbor spin correlation). Consequently, TPQ shows fast spectral convergence for most values of α (the parameter that drives the phase transition and interpolates between the Heisenberg and Kitaev models). CPGF shows similarly fast convergence (i.e. the number of polynomials needed to match ED results is of the same order) provided that the resolution is adjusted accordingly.

The resolution plays a central role when comparing the performance of the two approaches. In CPGF, finer resolutions always require more polynomials to achieve convergence and there is no reliable way to match the input resolution of CPGF to the effective resolution of TPQ (which varies as more iterations are completed). Nonetheless, we managed to compare the two methods by using ED as a control method. First, we focused on $\alpha \sim 0.8$ (close to the transition to the spin liquid state at $\alpha_c = 0.808$) and obtained close agreement with the ED results using both methods. Then, we examined their convergence properties. TPQ showed an erratic convergence speed, particularly for $\alpha = \alpha_c$, at which point CPGF converges faster. For the other points we

considered close to the transition, CPGF converges faster as $\alpha \rightarrow \alpha_c^+$ and slower as $\alpha \rightarrow \alpha_c^-$. Broadly speaking, close to the transition, around 30000-40000 polynomials/iterations are needed to achieve convergence and thus match the ED results satisfactorily. TPQ shows lower statistical fluctuations and considering 4 realizations seems to suffice to achieve negligible deviations from the exact diagonalization results for all values of α . CPGF shows higher fluctuations, particularly at the phase transition to the spin liquid state, in which case 40 – 60 random vectors are needed to produce negligibly small error bars. This also highlights the fact that a very fine resolution was needed to recover the ED results near the transition. On the other hand, away from quantum critical points, a comparatively coarse resolution is enough to reproduce the ED results and both methods show similar performance. Convergence is faster and a lower input resolution in CPGF suffices to match the results of ED.

Our results show a clear trade off that must be taken into account when choosing which method to use. TPQ is clearly designed to achieve maximum accuracy for the ground state. However, TPQ does not allow direct specification of the energy resolution, nor can it isolate excited states. The ensuing lack of control stems from the fact that expectation values are computed for a finite effective temperature in TPQ. Concomitantly, the additional control afforded by the CPGF approach — which can access excited states directly — could be useful for studying non equilibrium systems, such as those studied in Ref. [7].

A particularly relevant competing method is DMRG [23]. The idea of DMRG is to systematically truncate the exponentially large Hilbert space basis. The basis is rotated in the process in order to improve the accuracy of the truncation. This rotation is achieved via a series of global rotations generated by sweeping the lattice and thus focusing on a few sites at a time. The wide applicability of the DMRG procedure means that it can be used as a general purpose, sign problem free method to study 2D spin systems. Moreover, it yields results that are competitive with QMC. However, since DMRG was designed for 1D systems, it is more difficult to use DMRG in 2D and it is not as accurate as in 1D. CPGF is a potential alternative to DMRG because it poses no restrictions on dimensionality and its accuracy can be precisely controlled by ensuring statistical convergence and by adjusting the spectral resolution.

While CPGF has proven to be computationally intensive in the study of spin–correlations in the extended K-H model, it provides a general framework to investigate generic equilibrium and non-equilibrium properties (which, for example, TPQ is not designed for). Moreover, the observed differences in computational cost could be drastically reduced when studying other properties, such as long-range correlations, a point that is worthy of future study. Another important remark is that although we have used the ground state energy obtained with ED as an unbiased input for CPGF, Fig. 3 (left panel) clearly shows that the ground state energies from TPQ could have been used instead. Our findings therefore suggest a hybrid TPQ-CPGF approach to calculate generic low-temperature properties of quantum magnets: (i) first estimate the ground state energy with TPQ and (ii) then use the TPQ-estimated energy as an input to CPGF. Such an approach would avoid diagonalization, benefiting simultaneously from the strengths of TPQ (accurate estimate of the ground state energy) and CPGF (iterative reconstruction of generic observables with precisely defined energy resolution).

Acknowledgements

This project was undertaken on the Viking Cluster, which is a high performance computing facility provided by the University of York. We are grateful for computational support from the University of York High Performance Computing service (Viking) and the Research Computing team.

Funding information F. B. is supported by a DTP studentship funded by the Engineering and Physical Sciences Research Council. A.F. acknowledges financial support from the Royal Society through a Royal Society University Research Fellowship.

A Stochastic Trace Evaluation

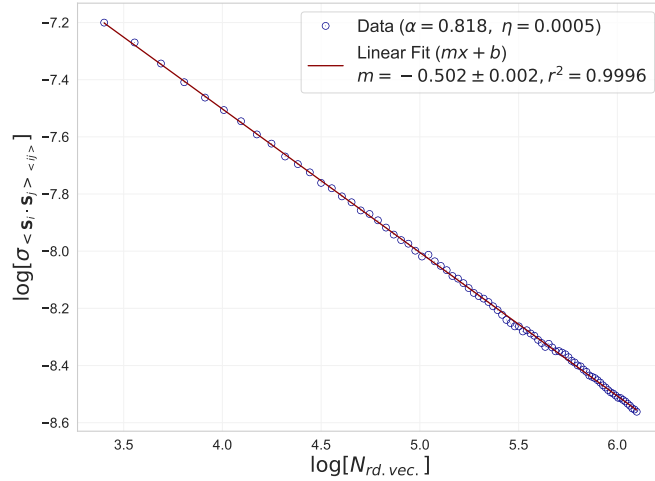


Figure 7: Standard deviation of the expectation value of the spin–spin correlation computed with CPGF for $\alpha = 0.818$ and resolution $\eta = 0.0005J_H$ as a function of the number of random vectors used in the computation of the expected value. The linear fit confirms the expected behavior: $\sigma \propto N_{\text{rd. vec.}}^{-1/2}$.

We evaluate the expectation value of the spin correlation using a stochastic approach. Statistical convergence is obtained when the error bars become acceptably small. This information is encoded in the scaling of the standard deviation with the number of used initial random states. In Fig. 7, we confirm that we obtain the expected scaling ($\sigma \propto N_{\text{rd. vec.}}^{-1/2}$) [41], that is our error bars can be made as small as required by simply averaging over more realizations of the initial random state.

References

- [1] L. D. Carr, *Understanding Quantum Phase Transitions*, CRC Press, 1 edn., doi:[10.1201/b10273](https://doi.org/10.1201/b10273) (2010).

- [2] S. Sachdev, *Quantum Phase Transitions*, Cambridge University Press, 2 edn., doi:[10.1017/CBO9780511973765](https://doi.org/10.1017/CBO9780511973765) (2011).
- [3] J. Chaloupka, G. Jackeli and G. Khaliullin, *Kitaev-Heisenberg Model on a Honeycomb Lattice: Possible Exotic Phases in Iridium Oxides A_2IrO_3* , Phys. Rev. Lett. **105**(2), 027204 (2010), doi:[10.1103/PhysRevLett.105.027204](https://doi.org/10.1103/PhysRevLett.105.027204).
- [4] C. C. Price and N. B. Perkins, *Critical Properties of the Kitaev-Heisenberg Model*, Phys. Rev. Lett. **109**, 187201 (2012), doi:[10.1103/PhysRevLett.109.187201](https://doi.org/10.1103/PhysRevLett.109.187201).
- [5] J. Nasu, M. Udagawa and Y. Motome, *Vaporization of Kitaev Spin Liquids*, Phys. Rev. Lett. **113**(19), 197205 (2014), doi:[10.1103/PhysRevLett.113.197205](https://doi.org/10.1103/PhysRevLett.113.197205).
- [6] J. Nasu, M. Udagawa and Y. Motome, *Thermal fractionalization of quantum spins in a Kitaev model: Temperature-linear specific heat and coherent transport of Majorana fermions*, Phys. Rev. B **92**(11), 115122 (2015), doi:[10.1103/PhysRevB.92.115122](https://doi.org/10.1103/PhysRevB.92.115122).
- [7] J. Nasu and Y. Motome, *Nonequilibrium Majorana dynamics by quenching a magnetic field in Kitaev spin liquids*, Phys. Rev. Research **1**(3), 033007 (2019), doi:[10.1103/PhysRevResearch.1.033007](https://doi.org/10.1103/PhysRevResearch.1.033007).
- [8] H. Li, D.-W. Qu, H.-K. Zhang, Y.-Z. Jia, S.-S. Gong, Y. Qi and W. Li, *Universal thermodynamics in the Kitaev fractional liquid*, Phys. Rev. Research **2**(4), 043015 (2020), doi:[10.1103/PhysRevResearch.2.043015](https://doi.org/10.1103/PhysRevResearch.2.043015).
- [9] C. Hickey, C. Berke, P. P. Stavropoulos, H.-Y. Kee and S. Trebst, *Field-driven gapless spin liquid in the spin-1 Kitaev honeycomb model*, Phys. Rev. Research **2**(2), 023361 (2020), doi:[10.1103/PhysRevResearch.2.023361](https://doi.org/10.1103/PhysRevResearch.2.023361).
- [10] H. Bethe, *Zur Theorie der Metalle*, Z. Physik **71**(3), 205 (1931), doi:[10.1007/BF01341708](https://doi.org/10.1007/BF01341708).
- [11] C. Lanczos, *An iteration method for the solution of the eigenvalue problem of linear differential and integral operators*, Journal of Research of the National Bureau of Standards **45**(4), 255 (1950), doi:[10.6028/jres.045.026](https://doi.org/10.6028/jres.045.026).
- [12] S. M. Winter, K. Riedl, D. Kaib, R. Coldea and R. Valentí, *Probing α - $RuCl_3$ Beyond Magnetic Order: Effects of Temperature and Magnetic Field*, Phys. Rev. Lett. **120**(7), 077203 (2018), doi:[10.1103/PhysRevLett.120.077203](https://doi.org/10.1103/PhysRevLett.120.077203).
- [13] M. Rigol, T. Bryant and R. R. P. Singh, *Numerical Linked-Cluster Approach to Quantum Lattice Models*, Phys. Rev. Lett. **97**(18), 187202 (2006), doi:[10.1103/PhysRevLett.97.187202](https://doi.org/10.1103/PhysRevLett.97.187202).
- [14] A. B. Kallin, K. Hyatt, R. R. P. Singh and R. G. Melko, *Entanglement at a Two-Dimensional Quantum Critical Point: A Numerical Linked-Cluster Expansion Study*, Phys. Rev. Lett. **110**(13), 135702 (2013), doi:[10.1103/PhysRevLett.110.135702](https://doi.org/10.1103/PhysRevLett.110.135702).
- [15] T. Devakul and R. R. Singh, *Early Breakdown of Area-Law Entanglement at the Many-Body Delocalization Transition*, Phys. Rev. Lett. **115**(18), 187201 (2015), doi:[10.1103/PhysRevLett.115.187201](https://doi.org/10.1103/PhysRevLett.115.187201).
- [16] R. Schäfer, I. Hagymási, R. Moessner and D. J. Luitz, *Pyrochlore $S = \frac{1}{2}$ Heisenberg antiferromagnet at finite temperature*, Phys. Rev. B **102**(5), 054408 (2020), doi:[10.1103/PhysRevB.102.054408](https://doi.org/10.1103/PhysRevB.102.054408).

- [17] J. Richter, T. Heitmann and R. Steinigeweg, *Quantum quench dynamics in the transverse-field Ising model: A numerical expansion in linked rectangular clusters*, SciPost Physics **9**(3), 031 (2020), doi:[10.21468/SciPostPhys.9.3.031](https://doi.org/10.21468/SciPostPhys.9.3.031).
- [18] I. Hagymási, R. Schäfer, R. Moessner and D. J. Luitz, *Possible Inversion Symmetry Breaking in the $S = 1/2$ Pyrochlore Heisenberg Magnet*, Phys. Rev. Lett. **126**(11), 117204 (2021), doi:[10.1103/PhysRevLett.126.117204](https://doi.org/10.1103/PhysRevLett.126.117204).
- [19] T. Kuwahara, A. M. Alhambra and A. Anshu, *Improved Thermal Area Law and Quasi-linear Time Algorithm for Quantum Gibbs States*, Phys. Rev. X **11**(1), 011047 (2021), doi:[10.1103/PhysRevX.11.011047](https://doi.org/10.1103/PhysRevX.11.011047).
- [20] E. Ghorbani, L. F. Tocchio and F. Becca, *Variational wave functions for the $S = \frac{1}{2}$ Heisenberg model on the anisotropic triangular lattice: Spin liquids and spiral orders*, Phys. Rev. B **93**(8), 085111 (2016), doi:[10.1103/PhysRevB.93.085111](https://doi.org/10.1103/PhysRevB.93.085111).
- [21] S. R. White, *Density matrix formulation for quantum renormalization groups*, Phys. Rev. Lett. **69**(19), 2863 (1992), doi:[10.1103/PhysRevLett.69.2863](https://doi.org/10.1103/PhysRevLett.69.2863).
- [22] U. Schollwöck, *The density-matrix renormalization group*, Rev. Mod. Phys. **77**(1), 259 (2005), doi:[10.1103/RevModPhys.77.259](https://doi.org/10.1103/RevModPhys.77.259).
- [23] E. M. Stoudenmire and S. R. White, *Studying Two Dimensional Systems With the Density Matrix Renormalization Group*, Annu. Rev. Condens. Matter Phys. **3**(1), 111 (2012), doi:[10.1146/annurev-conmatphys-020911-125018](https://doi.org/10.1146/annurev-conmatphys-020911-125018).
- [24] S. Sugiura and A. Shimizu, *Thermal Pure Quantum States at Finite Temperature*, Phys. Rev. Lett. **108**(24), 240401 (2012), doi:[10.1103/PhysRevLett.108.240401](https://doi.org/10.1103/PhysRevLett.108.240401).
- [25] S. Sugiura and A. Shimizu, *Canonical Thermal Pure Quantum State*, Phys. Rev. Lett. **111**(1), 010401 (2013), doi:[10.1103/PhysRevLett.111.010401](https://doi.org/10.1103/PhysRevLett.111.010401).
- [26] A. Wietek, P. Corboz, S. Wessel, B. Normand, F. Mila and A. Honecker, *Thermodynamic properties of the Shastry-Sutherland model throughout the dimer-product phase*, Phys. Rev. Research **1**(3), 033038 (2019), doi:[10.1103/PhysRevResearch.1.033038](https://doi.org/10.1103/PhysRevResearch.1.033038).
- [27] P. Laurell and S. Okamoto, *Dynamical and thermal magnetic properties of the Kitaev spin liquid candidate α - RuCl_3* , npj Quantum Materials **5**(1), 1 (2020), doi:[10.1038/s41535-019-0203-y](https://doi.org/10.1038/s41535-019-0203-y).
- [28] W.-J. Hu, S.-S. Gong and D. N. Sheng, *Variational Monte Carlo study of chiral spin liquid in quantum antiferromagnet on the triangular lattice*, Phys. Rev. B **94**(7), 075131 (2016), doi:[10.1103/PhysRevB.94.075131](https://doi.org/10.1103/PhysRevB.94.075131).
- [29] J. Wang, Q. Zhao, X. Wang and Z.-X. Liu, *Multinode quantum spin liquids on the honeycomb lattice*, Phys. Rev. B **102**(14), 144427 (2020), doi:[10.1103/PhysRevB.102.144427](https://doi.org/10.1103/PhysRevB.102.144427).
- [30] M. Troyer and U.-J. Wiese, *Computational Complexity and Fundamental Limitations to Fermionic Quantum Monte Carlo Simulations*, Phys. Rev. Lett. **94**(17), 170201 (2005), doi:[10.1103/PhysRevLett.94.170201](https://doi.org/10.1103/PhysRevLett.94.170201).

- [31] A. Kitaev, *Anyons in an exactly solved model and beyond*, Annals of Physics **321**(1), 2 (2006), doi:[10.1016/j.aop.2005.10.005](https://doi.org/10.1016/j.aop.2005.10.005).
- [32] G. H. Wannier, *Antiferromagnetism. The Triangular Ising Net*, Phys. Rev. **79**(2), 357 (1950), doi:[10.1103/PhysRev.79.357](https://doi.org/10.1103/PhysRev.79.357).
- [33] S. Trebst, *Kitaev Materials*, arXiv:1701.07056 [cond-mat] (2017), <http://arxiv.org/abs/1701.07056>.
- [34] M. Hermanns, I. Kimchi and J. Knolle, *Physics of the Kitaev Model: Fractionalization, Dynamic Correlations, and Material Connections*, Annu. Rev. Condens. Matter Phys. **9**(1), 17 (2018), doi:[10.1146/annurev-conmatphys-033117-053934](https://doi.org/10.1146/annurev-conmatphys-033117-053934).
- [35] D. Pesin and L. Balents, *Mott physics and band topology in materials with strong spin-orbit interaction*, Nature Physics **6**(5), 376 (2010), doi:[10.1038/nphys1606](https://doi.org/10.1038/nphys1606).
- [36] L. Balents, *Spin liquids in frustrated magnets*, Nature **464**(7286), 199 (2010), doi:[10.1038/nature08917](https://doi.org/10.1038/nature08917).
- [37] L. Savary and L. Balents, *Quantum spin liquids: a review*, Rep. Prog. Phys. **80**(1), 016502 (2016), doi:[10.1088/0034-4885/80/1/016502](https://doi.org/10.1088/0034-4885/80/1/016502).
- [38] P. A. Maksimov and A. L. Chernyshev, *Rethinking α -RuCl₃*, Phys. Rev. Research **2**(3), 033011 (2020), doi:[10.1103/PhysRevResearch.2.033011](https://doi.org/10.1103/PhysRevResearch.2.033011).
- [39] J. Nasu and Y. Motome, *Thermodynamic and transport properties in disordered Kitaev models*, Phys. Rev. B **102**(5), 054437 (2020), doi:[10.1103/PhysRevB.102.054437](https://doi.org/10.1103/PhysRevB.102.054437).
- [40] J. Nasu and Y. Motome, *Spin dynamics in the Kitaev model with disorder: Quantum Monte Carlo study of dynamical spin structure factor, magnetic susceptibility, and NMR relaxation rate*, Phys. Rev. B **104**(3), 035116 (2021), doi:[10.1103/PhysRevB.104.035116](https://doi.org/10.1103/PhysRevB.104.035116).
- [41] A. Weisse, G. Wellein, A. Alvermann and H. Fehske, *The kernel polynomial method*, Rev. Mod. Phys. **78**(1), 275 (2006), doi:[10.1103/RevModPhys.78.275](https://doi.org/10.1103/RevModPhys.78.275).
- [42] J. H. García, L. Covaci and T. G. Rappoport, *Real-Space Calculation of the Conductivity Tensor for Disordered Topological Matter*, Phys. Rev. Lett. **114**(11), 116602 (2015), doi:[10.1103/PhysRevLett.114.116602](https://doi.org/10.1103/PhysRevLett.114.116602).
- [43] T. P. Cysne, T. G. Rappoport, A. Ferreira, J. M. V. P. Lopes and N. M. R. Peres, *Numerical calculation of the Casimir-Polder interaction between a graphene sheet with vacancies and an atom*, Phys. Rev. B **94**(23), 235405 (2016), doi:[10.1103/PhysRevB.94.235405](https://doi.org/10.1103/PhysRevB.94.235405).
- [44] M. Mashkoori, K. Björnson and A. M. Black-Schaffer, *Impurity bound states in fully gapped d -wave superconductors with subdominant order parameters*, Scientific Reports **7**(1) (2017), doi:[10.1038/srep44107](https://doi.org/10.1038/srep44107).
- [45] J. L. Lado and O. Zilberberg, *Topological spin excitations in Harper-Heisenberg spin chains*, Phys. Rev. Research **1**(3), 033009 (2019), doi:[10.1103/PhysRevResearch.1.033009](https://doi.org/10.1103/PhysRevResearch.1.033009).
- [46] J. L. Lado and M. Sgrist, *Solitonic in-gap modes in a superconductor-quantum antiferromagnet interface*, Phys. Rev. Research **2**(2), 023347 (2020), doi:[10.1103/PhysRevResearch.2.023347](https://doi.org/10.1103/PhysRevResearch.2.023347).

- [47] D. Varjas, M. Fruchart, A. R. Akhmerov and P. M. Perez-Piskunow, *Computation of topological phase diagram of disordered $Pb_{1-x}Sn_xTe$ using the kernel polynomial method*, Phys. Rev. Research **2**(1), 013229 (2020), doi:[10.1103/PhysRevResearch.2.013229](https://doi.org/10.1103/PhysRevResearch.2.013229).
- [48] S. M. João and J. M. Viana Parente Lopes, *Basis-independent spectral methods for non-linear optical response in arbitrary tight-binding models*, J. Phys.: Condens. Matter **32**(12), 125901 (2020), doi:[10.1088/1361-648X/ab59ec](https://doi.org/10.1088/1361-648X/ab59ec).
- [49] V. Kaskela and J. L. Lado, *Dynamical topological excitations in parafermion chains*, Phys. Rev. Research **3**(1), 013095 (2021), doi:[10.1103/PhysRevResearch.3.013095](https://doi.org/10.1103/PhysRevResearch.3.013095).
- [50] M. Rösner and J. L. Lado, *Inducing a many-body topological state of matter through Coulomb-engineered local interactions*, Phys. Rev. Research **3**(1), 013265 (2021), doi:[10.1103/PhysRevResearch.3.013265](https://doi.org/10.1103/PhysRevResearch.3.013265).
- [51] J. P. S. Pires, B. Amorim, A. Ferreira, Í. Adagideli, E. R. Mucciolo and J. M. V. P. Lopes, *Breakdown of universality in three-dimensional Dirac semimetals with random impurities*, Phys. Rev. Research **3**(1), 013183 (2021), doi:[10.1103/PhysRevResearch.3.013183](https://doi.org/10.1103/PhysRevResearch.3.013183).
- [52] T. Löthman, C. Triola, J. Cayao and A. M. Black-Schaffer, *Efficient numerical method for evaluating normal and anomalous time-domain equilibrium Green's functions in inhomogeneous systems*, Phys. Rev. B **104**(12), 125405 (2021), doi:[10.1103/PhysRevB.104.125405](https://doi.org/10.1103/PhysRevB.104.125405).
- [53] T. Löthman, C. Triola, J. Cayao and A. M. Black-Schaffer, *Disorder-robust p-wave pairing with odd-frequency dependence in normal metal-conventional superconductor junctions*, Physical Review B **104**(9), 094503 (2021), doi:[10.1103/PhysRevB.104.094503](https://doi.org/10.1103/PhysRevB.104.094503).
- [54] A. Ferreira and E. R. Mucciolo, *Critical Delocalization of Chiral Zero Energy Modes in Graphene*, Phys. Rev. Lett. **115**(10), 106601 (2015), doi:[10.1103/PhysRevLett.115.106601](https://doi.org/10.1103/PhysRevLett.115.106601).
- [55] A. Braun and P. Schmitteckert, *Numerical evaluation of Green's functions based on the Chebyshev expansion*, Phys. Rev. B **90**(16), 165112 (2014), doi:[10.1103/PhysRevB.90.165112](https://doi.org/10.1103/PhysRevB.90.165112).
- [56] S. M. João, M. Andelković, L. Covaci, T. G. Rappoport, J. M. V. P. Lopes and A. Ferreira, *KITE: high-performance accurate modelling of electronic structure and response functions of large molecules, disordered crystals and heterostructures*, Royal Society Open Science **7**(2), 191809 (2020), doi:[10.1098/rsos.191809](https://doi.org/10.1098/rsos.191809).
- [57] T. Iitaka and T. Ebisuzaki, *Random phase vector for calculating the trace of a large matrix*, Phys. Rev. E **69**, 057701 (2004), doi:[10.1103/PhysRevE.69.057701](https://doi.org/10.1103/PhysRevE.69.057701).
- [58] S. Okamoto, G. Alvarez, E. Dagotto and T. Tohyama, *Accuracy of the microcanonical Lanczos method to compute real-frequency dynamical spectral functions of quantum models at finite temperatures*, Phys. Rev. E **97**(4), 043308 (2018), doi:[10.1103/PhysRevE.97.043308](https://doi.org/10.1103/PhysRevE.97.043308).
- [59] J. Schnack, J. Richter and R. Steinigeweg, *Accuracy of the finite-temperature Lanczos method compared to simple typicality-based estimates*, Phys. Rev. Research **2**(1), 013186 (2020), doi:[10.1103/PhysRevResearch.2.013186](https://doi.org/10.1103/PhysRevResearch.2.013186).
- [60] J. P. Boyd, *Chebyshev & Fourier Spectral Methods*, Lecture Notes in Engineering. Springer-Verlag, Berlin Heidelberg, ISBN 978-3-540-51487-9 (1989).

- [61] A. Catuneanu, Y. Yamaji, G. Wachtel, Y. B. Kim and H.-Y. Kee, *Path to stable quantum spin liquids in spin-orbit coupled correlated materials*, npj Quant Mater **3**(1), 1 (2018), doi:[10.1038/s41535-018-0095-2](https://doi.org/10.1038/s41535-018-0095-2).
- [62] H.-C. Jiang, H. Yao and L. Balents, *Spin liquid ground state of the spin- $\frac{1}{2}$ square J_1 - J_2 Heisenberg model*, Phys. Rev. B **86**(2), 024424 (2012), doi:[10.1103/PhysRevB.86.024424](https://doi.org/10.1103/PhysRevB.86.024424).
- [63] S. Depenbrock, I. P. McCulloch and U. Schollwöck, *Nature of the Spin-Liquid Ground State of the $S = 1/2$ Heisenberg Model on the Kagome Lattice*, Phys. Rev. Lett. **109**(6), 067201 (2012), doi:[10.1103/PhysRevLett.109.067201](https://doi.org/10.1103/PhysRevLett.109.067201).
- [64] J. Becker and S. Wessel, *Diagnosing Fractionalization from the Spin Dynamics of Z_2 Spin Liquids on the Kagome Lattice by Quantum Monte Carlo Simulations*, Phys. Rev. Lett. **121**(7), 077202 (2018), doi:[10.1103/PhysRevLett.121.077202](https://doi.org/10.1103/PhysRevLett.121.077202).
- [65] T. Sato and F. F. Assaad, *Quantum Monte Carlo simulation of generalized Kitaev models*, Phys. Rev. B **104**(8), L081106 (2021), doi:[10.1103/PhysRevB.104.L081106](https://doi.org/10.1103/PhysRevB.104.L081106).